

## Supporting Information

### Investigation on the Role of Amines in the Liquefaction and Recrystallization process of MAPbI<sub>3</sub> perovskite

Xi Yuan Feng,<sup>a, b, †</sup> Kar Wei Ng,<sup>a, c, †</sup> Shuang Peng Wang,<sup>a, c</sup> \* Wen Zhou Chen,<sup>a</sup> Zhen Zhong Zhang,<sup>d</sup>  
Wei Chen,<sup>b</sup> Yun Yang Zhao,<sup>a</sup> Bao Tu,<sup>a, b</sup> Zi Kang Tang,<sup>a, c</sup> Hui Pan,<sup>a, c</sup> \* Zhu Bing He,<sup>b, \*</sup>

<sup>a</sup>Joint Key Laboratory of the Ministry of Education, Institute of Applied Physics and Materials Engineering, University of Macau, Avenida da Universidade, Taipa, Macau, China

<sup>b</sup>Department of Materials Science and Engineering, Shenzhen Key Laboratory of Full Spectral Solar Electricity Generation (FSSEG), Southern University of Science and Technology, No. 1088, Xueyuan Rd., Shenzhen, China

<sup>c</sup>Department of Physics and Chemistry, Faculty of Science and Technology, University of Macau, Avenida da Universidade, Taipa, Macau, China

<sup>d</sup>State Key Laboratory of Luminescence and Applications, Changchun Institute of Optics, Fine Mechanics and Physics, Chinese Academy of Sciences, No.3888 Dongnanhu Road, Changchun, China

<sup>†</sup> These authors contributed equally to this work.

\*Corresponding authors: [spwang@umac.mo](mailto:spwang@umac.mo); [hez@ustc.edu.cn](mailto:hez@ustc.edu.cn)

<sup>†</sup>Xi Yuan Feng and Kar Wei Ng contribute equally to this work

**Keywords:** Amine; liquefaction; recrystallization; MAPbI<sub>3</sub>; Pb recycling; Perovskite solar cell

## Thoughts and organization of data to illustrate the reversible liquefaction of MPI perovskite

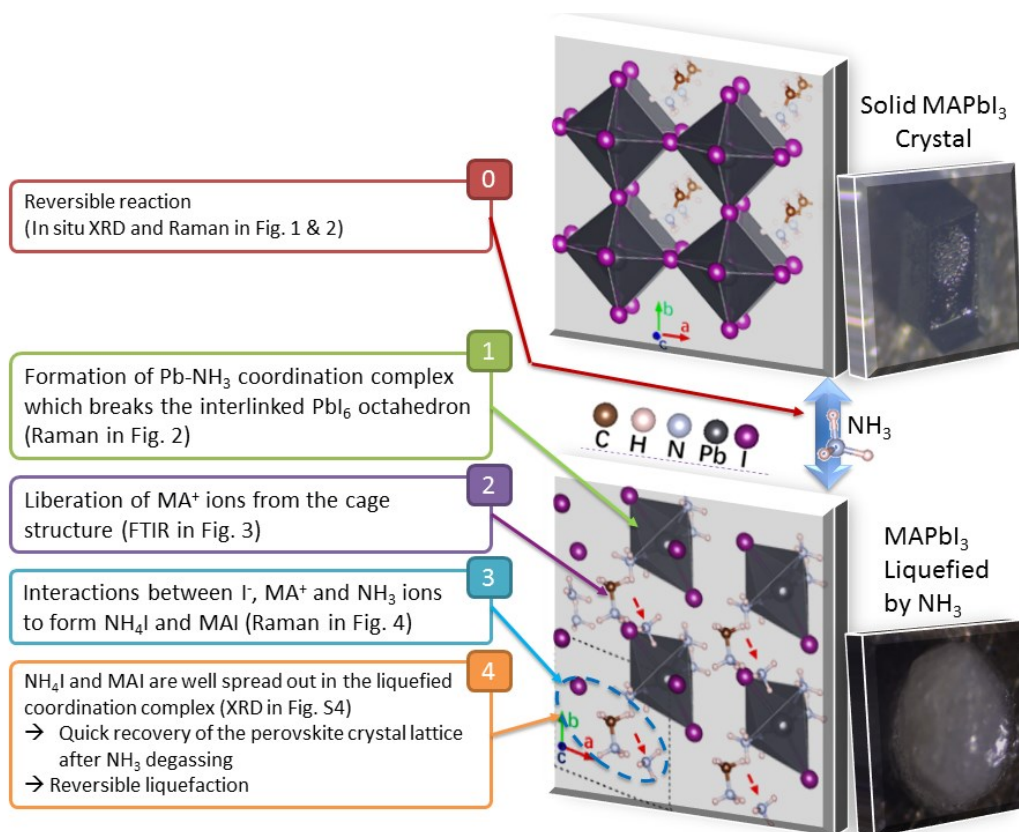


## **Table of Contents**

- 1. Materials**
- 2. XRD measurement**
- 3. Fourier Transform Infrared (FTIR) Spectrum measurement**
- 4. In-situ Raman Spectrum measurement**
- 5. Fabrication process and performance of perovskite solar cell**
- 6. Fabrication of  $\text{NH}_4\text{PbI}_3$  and  $\text{BA}_2\text{PbI}_4$  film**
- 7. Preparation of solid-state sample of  $\text{NH}_3$  treated MPI**
- 8. Computational methods and results**
- 9. References**

## 1. Materials

CH<sub>3</sub>NH<sub>3</sub>I (MAI), CH<sub>3</sub>CH<sub>2</sub>CH<sub>2</sub>CH<sub>2</sub>NH<sub>3</sub>I (BAI) and PbI<sub>2</sub> were purchased from Xi'an polymer Light Technology Corporation and were used without further process. NH<sub>4</sub>I was purchased from Shanghai Aladdin Bio-Chem Technology Co.,LTD. PCBM and BCP was purchased from Lumtec. The anhydrous solvents including N,N-dimethylformamide (DMF, 99.8%), dimethyl sulfoxide (DMSO, 99.8%), isopropanol (IPA, 99.8%), chlorobenzene (CB, 99.8%), Hydriodic acid (57wt.% solution in H<sub>2</sub>O) and ethylene glycol purchased from Acros Organics. Ethylenediamine (99.5%) and methylamine (MA)-ethanol(33% wt) solution was purchased from Sigma. Ammonia water (20% wt), ammonia-IPA solution (2M), ethylamine (EA)-ethanol (30%) solution and butylamine (BA) (99%) was purchased from 9dingchem. NH<sub>3</sub> gas (99.995%) was purchased from Wench technology in Shenzhen. Ni(NO<sub>3</sub>)<sub>2</sub>·6H<sub>2</sub>O was purchased from Alfa. MPI Single crystals were grown in solution via the temperature-lowering (TL) method as described in our previous work.<sup>1</sup>

## 2. XRD measurements

The XRD measurements were carried out in a Rigaku Smart Lab system. The in-situ XRD measurements are realized by a home-made measurement setup (shown in Figure S1d), the samples are sealed into the setup by APIEZON AP100. There is a sealed pin hole at the sidewall of the setup (shown in Figure S1d) for gas injection. To confirm the functionality of the setup for in-situ XRD, we employed a silicon (100) wafer as a reference. As shown in Figure S1a, the polymer cover does not cause any observable

peak shift or additional peak in the range from 10° to 70°. Powder XRD spectra of pristine MPI (shown in Figure S1b in black line) were measured at room temperature in air. There are nine diffraction peaks located at 14.04°, 19.88°, 23.42°, 24.24°, 28.38°, 31.80°, 34.88°, 40.40°, 42.98° and 50.12°, which can be attributed to the 110, 112, 211, 202, 220, 310, 312, 224, 314 and 404 diffractions of MPI crystal in the  $I_4cm$  space group of the tetragonal family, respectively.<sup>2-5</sup>

The process of the in-situ XRD measurement: The sample was firstly loaded into the measurement setup in nitrogen filled glove box, then the setup is mounted on the Smartlab system, Rigaku Co, Ltd. Japan (Figure S1c). About 1ml of the ammonia was injected into sealed mini compartment through the pin hole at the side wall, then the measurement was started. The XRD scan with the ranging from 10° to 60° was taken in every 3 min. The XRD patterns can be seen in Figure 1g.

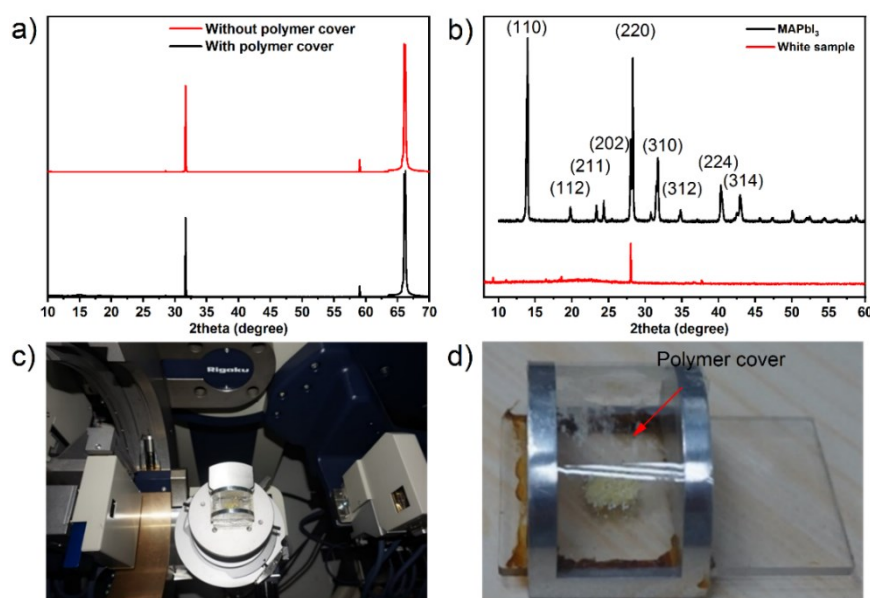


**Figure S1.** (a) Comparison of XRD spectrum of silicon with and without polymer cover in the setup, the spectra are almost the same, which indicates the home-made setup has

no effect on XRD measurements. (b) XRD pattern of pristine MPI perovskite powder and  $\text{NH}_3$  treated perovskite (the white sample show in (d)), (c) the setup mounted in the Rigaku Smartlab 9000W XRD system and (d) the *in situ* XRD measurement setup with a white sample. The white sample is the product of MPI powder exposed in  $\text{NH}_3$  for 96 h.

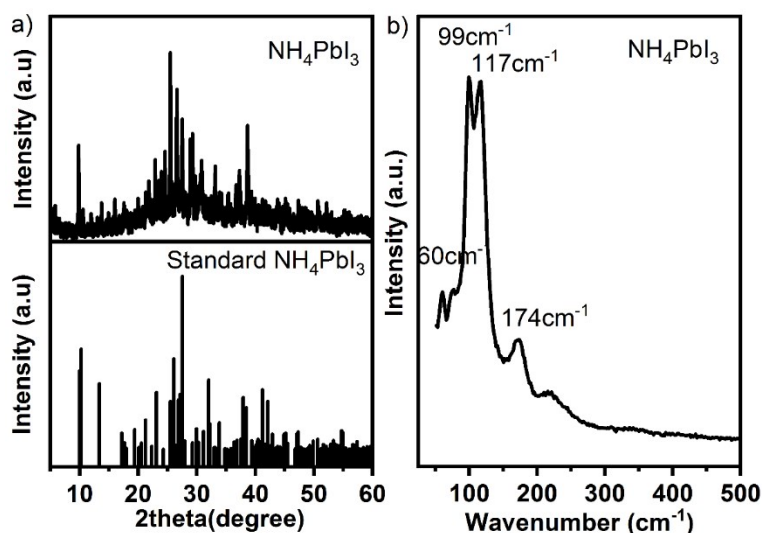


**Figure S2.** (a) XRD and (b) Raman spectra of  $\text{NH}_4\text{PbI}_3$  film, the Raman spectrum of  $\text{NH}_4\text{PbI}_3$  is very different from the  $\text{NH}_3$  treated MPI. It implies the  $\text{NH}_4\text{PbI}_3$  is not the product of  $\text{NH}_3$  treated MPI in our experiment.

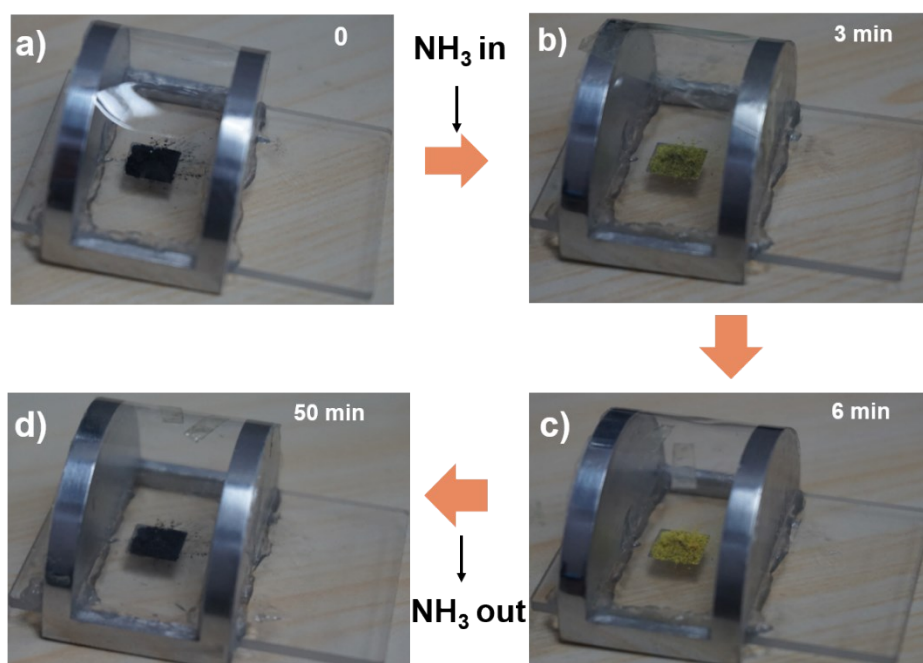


**Figure S3.** (a)-(d) The evolution of MPI sample with  $\text{NH}_3$  treatment in the *in situ* XRD measurement setup.

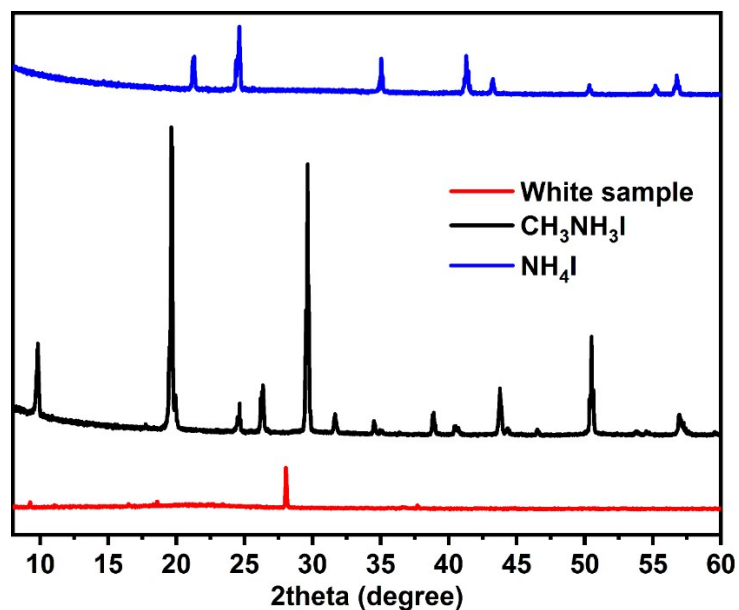


**Figure S4.** XRD spectra of solidified MPI upon exposure to  $\text{NH}_3$  for over 96 h (white sample),  $\text{CH}_3\text{NH}_3\text{I}$  powder and  $\text{NH}_4\text{I}$  powder. The three spectra are completely different from one another, confirming that the solidified sample does not contain the conventional phases of  $\text{NH}_4\text{I}$  and  $\text{CH}_3\text{NH}_3\text{I}$ .

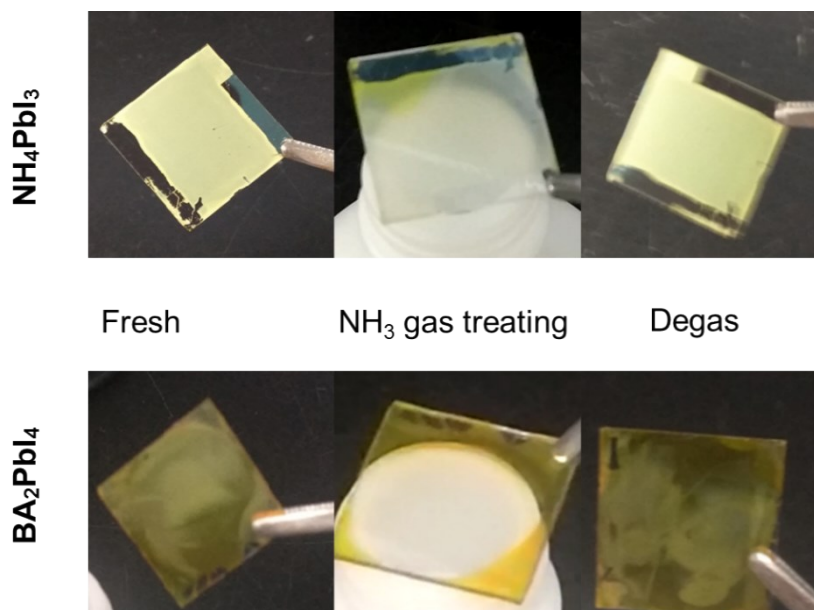


**Figure S5.** In order to illustrate the reversibility of  $\text{NH}_4\text{PbI}_3$  and  $\text{BA}_2\text{PbI}_4$  upon  $\text{NH}_3$ , fresh,  $\text{NH}_3$  gas treating and degassed process was shown.

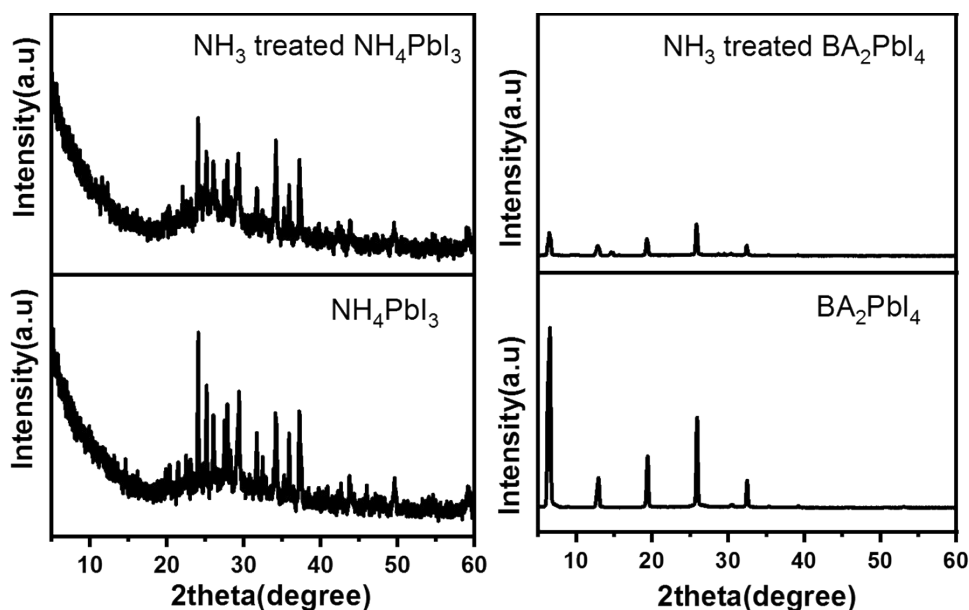


**Figure S6.** XRD pattern before and after  $\text{NH}_3$  treatment of  $\text{NH}_4\text{PbI}_3$  and  $\text{BA}_2\text{PbI}_4$

### 3. Fourier Transform Infrared Spectroscopy measurement

Samples were kept in a chamber with ammonia inside to create an ammonia environment, in which the sample can remain yellow before testing. During the measurement, the liquefied sample was transferred quickly onto the sample holder of the ATR accessory and infrared spectra were collected within 16 seconds by a Bruker VERTEX 70 FTIR Spectrometer with an ATR accessory ranging from 4000 to 400  $\text{cm}^{-1}$  before the sample turned to black.

### 4. In-situ Raman Spectrum measurement

Confocal Laser Raman Spectrometer (Horiba Lab RAM HR Evolution) was used to collect Raman signals. A 473nm solid-state laser was used as the excitation. An environment stage was employed. The MPI single crystal sample was firstly loaded into the environment stage in a nitrogen filled glovebox, after injection of  $\text{NH}_3$  into the stage,

the Raman measurement was started. In-situ Raman spectra were obtained in the range of 50 to 500  $\text{cm}^{-1}$ .

## 5. Fabrication process and performance of perovskite solar cell

The ITO/ $\text{NiO}_x$ /MPI/PCBM/BCP/Ag structured MPI solar cells were employed to test if the liquefaction of MPI can be used to recycle the parts of the solar cells and efficiently collect the lead containing full MPI based solar cells. In this demonstration, we focus on recycling the hole transport layer coated transparent conductive substrate (ITO/ $\text{NiO}_x$ ), which are considered as the first cost in a solar cell.

**Synthesis of  $\text{NiO}_x$  gel for  $\text{NiO}_x$  thin film:** 1.0 mmol  $\text{Ni}(\text{NO}_3)_2 \cdot 6\text{H}_2\text{O}$  was dissolved in 1 mL ethylene glycol. After the solution was stirred at room temperature for 20 min, 67  $\mu\text{L}$  ethylenediamine was added to the solution, and then the solution was further stirred 5 h at room temperature.

**Device Fabrication:** The pre-patterned indium tin oxide (ITO) coated glass substrates ( $2.5 \times 2.5 \text{ cm}^2$ ) were sequentially ultrasonic cleaned with detergent, deionized water, acetone, and isopropanol (IPA) for 15 min, respectively. Then, the substrates were dried with nitrogen gas and treated in a UV ozone oven for 15 min. A thin layer of  $\text{NiO}_x$  was spin coated on the substrates at 5000 rpm for 60 s and annealed at 300  $^\circ\text{C}$  for 50 min. After that, the substrates were transferred into a nitrogen-filled glove box. As the precursor for perovskite layer,  $\text{PbI}_2$  (1 mol) and MAI (1 mol) were dissolved in 1 mL mixed solvent of DMF and DMSO (v:v = 7:3) and stirred for 4 h at 60  $^\circ\text{C}$ . The perovskite precursor were then spin coated on top of  $\text{NiO}_x$  thin film at 3000

rpm for 35 s and 300  $\mu\text{L}$  chlorobenzene (CB) were dripped at the 25<sup>th</sup> second during the spin coating process. Then, the substrates were annealed at 100  $^{\circ}\text{C}$  for 15 min. Then, a layer of PCBM (20  $\text{mg mL}^{-1}$  in CB) was spin coated on top of the MPI layer at 1400 rpm for 30 s. After that, a layer of 8 nm BCP were deposited on the top of the PCBM layer by spin coating (5  $\text{mg mL}^{-1}$  in IPA). The devices were finished after thermally evaporating Ag of 100 nm. All the devices were confined by the metal mask with effective area of 7.5  $\text{mm}^2$ . A control device with a PCE of 18.28% was achieved. The performance of devices is shown in Figure S7 (a) while the device structure can be found in Figure S7 (e).

As shown in Figure S7(c), when the MPI solar cell is placed into water, the function layers almost cannot be dissolved. But when ammonia take part in the process, it is found that the MPI layer was totally dissolved in ammonia water in 20 min, while the superstructure (PCBM and Al in our device) could be easily removed and a clean  $\text{NiO}_x$  coated ITO glass substrate was acquired (Figure S7(d)), which could be contributed to the help of the liquefaction process from ammonia. The  $\text{NiO}_x$  coated ITO substrate was collected and the lead containing waste could be stored for further recycling process which would be reported elsewhere. To test the performance of the recycled substrate, MPI layer and other functional layers were deposited onto the recycled substrate successively in normal procedure to form the solar cell with reused substrate, a PCE of 17.83% was achieved in this device.( Figure S7 b), which is similar with the control device.

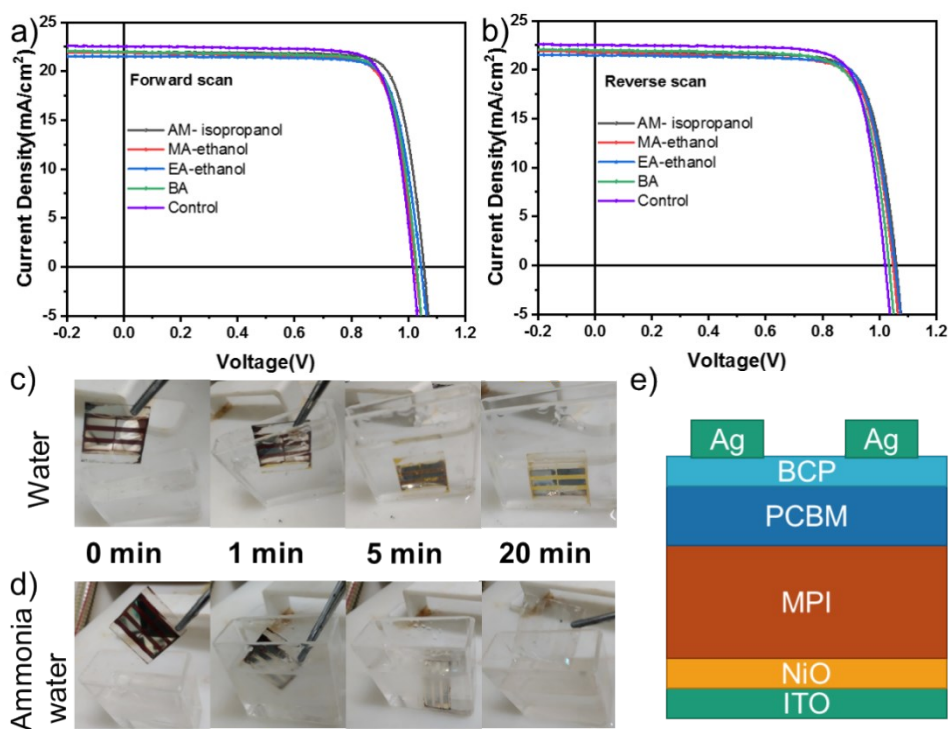


**Figure S7.** a) Forward scan and b) reverse scan of the I-V curves of devices fabricated upon reused substrates which were recollected by ammonia (AM)-isopropanol, methylamine-ethanol, ethylamine-ethanol and butylamine solutions. To collect substrate c) in water and d) in ammonia water, finally a substrate treated in ammonia water only could be collected and reused. e) Schematic of the device structure: ITO/NiO<sub>x</sub>/MPI/PCBM/BCP/Ag.

Solvents	Devices	J <sub>sc</sub>	V <sub>oc</sub> [V]	FF	PCE
		[mA cm <sup>-2</sup> ]		[%]	[%]
Control	Forward scan	22.53	1.02	79.5	18.28
	Reverse scan	22.50	1.02	78.6	18.03
AM-isopropanol	Forward scan	22.00	1.03	79.8	18.07
	Reverse scan	22.00	1.03	76.7	17.37
MA-ethanol	Forward scan	21.91	1.03	78.7	17.77

EA-ethanol	Reverse scan	21.75	1.05	76.9	17.55
	Forward scan	21.51	1.04	80.3	17.95
BA	Reverse scan	21.47	1.05	79.4	17.90
	Forward scan	22.00	1.03	79.8	18.07
	Reverse scan	22.00	1.03	76.7	17.37

**Table S1.** . Device performance parameters of the devices fabricated upon reused substrates which were recollected by ammonia (AM)-isopropanol, methylamine (MA)-ethanol, ethylamine(EA)-ethanol and butylamine(BA) solutions.

## 6. Fabrication of $\text{NH}_4\text{PbI}_3$ and $\text{BA}_2\text{PbI}_4$ film

### *$\text{NH}_4\text{PbI}_3$ film*

1 mmol of  $\text{NH}_4\text{I}$  and  $\text{PbI}_2$  were dissolved into 1ml of DMF respectively as the precursors. The precursors were then spin-coated at 3000 rpm for 30s on an ITO/glass substrate, followed by annealing at  $100^\circ\text{C}$  for 10 mins.

### *$\text{BA}_2\text{PbI}_4$ film*

2 mmol of BAI and 1mmol  $\text{PbI}_2$  were dissolved into 1ml of DMF respectively as the precursors. The precursors were then spin-coated at 3000 rpm for 30 s on an ITO/glass substrate, followed by annealing at  $100^\circ\text{C}$  for 10 mins.

## 7. Preparation of solid-state sample of $\text{NH}_3$ treated MPI

Put a crystal sample with size of 3 mm\*3 mm\*3 mm into a little bottle (4mL). Ammonia gas is injected into the bottle to remove other gases. Then keep the bottle sealed for 48hour or 96hour, the yellow and white sample will be prepared.

## 8. Computational methods and results

First-principles calculations were performed within the Vienna Ab initio Simulation Package (VASP),<sup>6</sup> based on the Density Functional Theory (DFT). The projector augmented wave (PAW) method,<sup>7</sup> was employed to describe the interactions between the ionic cores and valence electrons, with the valence electrons employed as  $6s^26p^2$ ,  $5s^25p^5$ ,  $2s^22p^3$ ,  $2s^22p^2$ , and  $1s^1$  for Pb, I, N, C, and H respectively. The correlation and exchange interactions were described by the generalized gradient approximation (GGA) parametrization of Perdew-Burke-Ernzerhof (PBE) functionals.<sup>8</sup> The value of Gaussian smearing was set to 0.05 eV. The convergence criteria for the electronic and ionic relaxations were set to  $1 \times 10^{-4}$  eV and  $0.01$  eV/Å, respectively. The k-points was sampled with a  $6 \times 6 \times 6$  grid centered at the Gamma by the Monkhorst-Pack method,<sup>9</sup> and the plane wave cutoff was set to 500 eV.

To model the MPI-n(NH<sub>3</sub>) systems, the NH<sub>3</sub> molecule is initially put in the center of the tetrahedra formed by three I and one Pb atoms, with N atom pointing to the Pb atom (Figure S8). The initial structures of the MPI-n(NH<sub>3</sub>) are then fully relaxed until the force acting on each atom and the total energy of the system converge to within 0.01 eV/Å and  $1 \times 10^{-4}$  eV, respectively. The relaxed structure of MPI show slightly structural distortion away from the perfect cubic perovskite and the average of lattice constant is predicted to be 6.446 Å, consistent with other reported value (6.431 Å) based on the DFT calculations,<sup>10</sup> indicating the validation of our calculations. For the cubic perovskite MPI, each Pb atom is surround by six I atoms forming the octahedra PbI<sub>6</sub>, which form chemical bond with their neighboring octahedra through the I atoms along

the three dimensions (Figure S9). Upon  $\text{NH}_3$  molecules intercalation, the relaxed structures of the  $\text{MPI-nNH}_3$  systems show that some I atoms are substituted by  $\text{NH}_3$  molecules, leading to the octahedra  $\text{PbI}_{(6-n)}(\text{NH}_3)_n$ . Compared to the octahedra  $\text{PbI}_6$ , the octahedra  $\text{PbI}_{(6-n)}(\text{NH}_3)_n$  present relatively weak interactions with their neighboring octahedra. For example, as  $n = 1$ , the neighboring octahedra  $\text{PbI}_5(\text{NH}_3)$  bond with each other through the I atoms and arrange periodically along b and c directions (Figure S10a and S10c), whereas they separate with each other along a direction (Figure S10b) with distance of 2.798 Å (Table S2). This separation is much larger than the sum of atomic radii of the I and H atoms (1.680 Å)<sup>11</sup>, suggesting their non-chemical bonding. On the other hand, it is slightly shorter than the sum of Van der Waals radii of the I and H atoms (3.180 Å)<sup>11</sup>, indicating the weak interaction between the neighboring octahedra  $\text{PbI}_5(\text{NH}_3)$  along a direction for the  $\text{MPI-1}(\text{NH}_3)$  system. For  $n = 2$ , we find that the neighboring octahedra  $\text{PbI}_4(\text{NH}_3)_2$  bond together through the I atoms along b direction (Figure S11c), whereas they interact relatively weak with distance of 2.903 and 2.859 Å along a and c directions (Figure S11a and S11b), respectively. As  $n \geq 3$ , the neighboring octahedra  $\text{PbI}_{(6-n)}(\text{NH}_3)_n$  interact with each other along all the three dimensions (Figure S12-14), because of their large separation (Table S2).

We see that the  $\text{MPI-n}(\text{NH}_3)$  systems could have two possible phases, due to the dependent of interactions between the neighboring octahedra  $\text{PbI}_{(6-n)}(\text{NH}_3)_n$  upon  $\text{NH}_3$  molecules insertion. For  $n = 1$  and  $n = 2$ , there exist both strong chemical bonding and weak interactions (or Van der Waals interactions) between the neighboring octahedra

$\text{PbI}_{(6-n)}(\text{NH}_3)_n$ . The weak interactions are unstable again by thermal fluctuation, and the MPI-1( $\text{NH}_3$ ) and MPI-2( $\text{NH}_3$ ) systems could become semi-liquid state at room temperature, because of the vanish of the weak interactions. For  $n \geq 3$ , the neighboring octahedra  $\text{PbI}_{(6-n)}(\text{NH}_3)_n$  interact with each other purely through weak interactions which could be destroyed by thermal fluctuation. Consequently, the MPI-n( $\text{NH}_3$ ) ( $n \geq 3$ ) systems could become liquid state at room temperature. These results are consistent with our experimental observation where the cubic perovskite MPI experience two phases upon  $\text{NH}_3$  molecules insertion. Furthermore, the interaction between the neighboring octahedra  $\text{PbI}_{(6-n)}(\text{NH}_3)_n$  are much weaker than that of the octahedra  $\text{PbI}_6$ , potentially leading to smaller Raman peaks. This is also consistent with our experimental finding, where the Raman peaks of cubic perovskite MPI decrease upon  $\text{NH}_3$  molecules intercalation.

**Table S2.** The calculated distance between the neighboring octahedra  $\text{PbI}_{(6-n)}(\text{NH}_3)_n$  along the a, b and c directions for the  $\text{MAPbI}_{3-n}(\text{NH}_3)_n$  systems. The separation is determined by either the distance between the I and H atoms, or the distance between the H and H atoms. The atomic radii of the I and H atoms are 1.150 and 0.530 Å,<sup>11</sup> respectively, whereas the Van der Waals radii of the I and H atoms are 1.980 and 1.200 Å,<sup>11</sup> respectively.

System	Octahedra	Distance of the neighboring octahedra (Å)		
		along a direction	along b direction	along c direction
MPI-1( $\text{NH}_3$ )	$\text{PbI}_5(\text{NH}_3)_1$	2.798 (I-H)	-	-

<b>MPI-2(NH<sub>3</sub>)</b>	PbI <sub>4</sub> (NH <sub>3</sub> ) <sub>2</sub>	2.903 (I-H)	-	2.859 (I-H)
<b>MPI-3(NH<sub>3</sub>)</b>	PbI <sub>3</sub> (NH <sub>3</sub> ) <sub>3</sub>	2.750 (I-H)	2.975 (I-H)	2.797 (I-H)
<b>MPI-4(NH<sub>3</sub>)</b>	PbI <sub>2</sub> (NH <sub>3</sub> ) <sub>4</sub>	2.610 (I-H)	2.761 (I-H)	4.569 (H-H)
<b>MPI-5(NH<sub>3</sub>)</b>	PbI <sub>2</sub> (NH <sub>3</sub> ) <sub>4</sub>	2.841 (I-H)	2.892 (I-H)	4.362 (H-H)

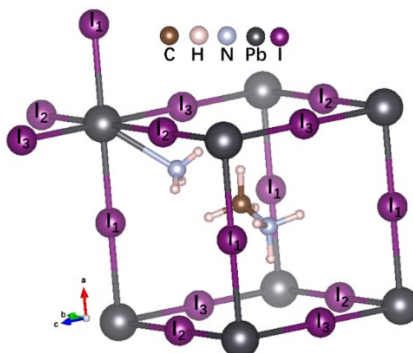


**Figure S8.** The crystal structure of cubic perovskite MPI upon one NH<sub>3</sub> molecule insertion.

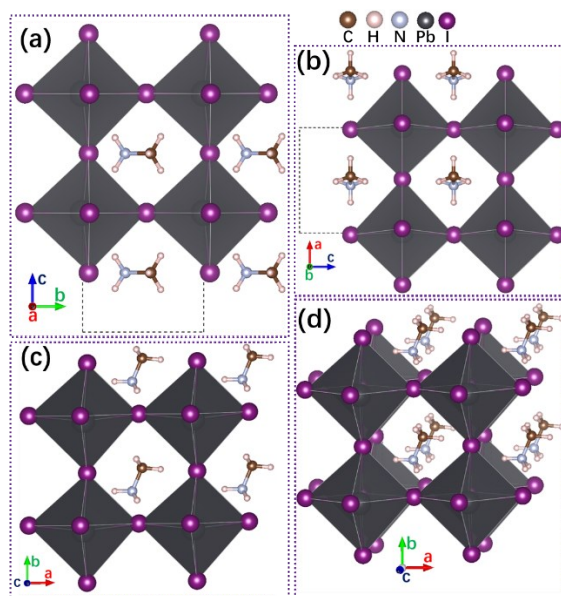


**Figure S9.** Structure of cubic perovskite MPI. Panel (a), (b) and (c) are top views from the *a*, *b* and *c* directions, respectively; (d) tilted view.

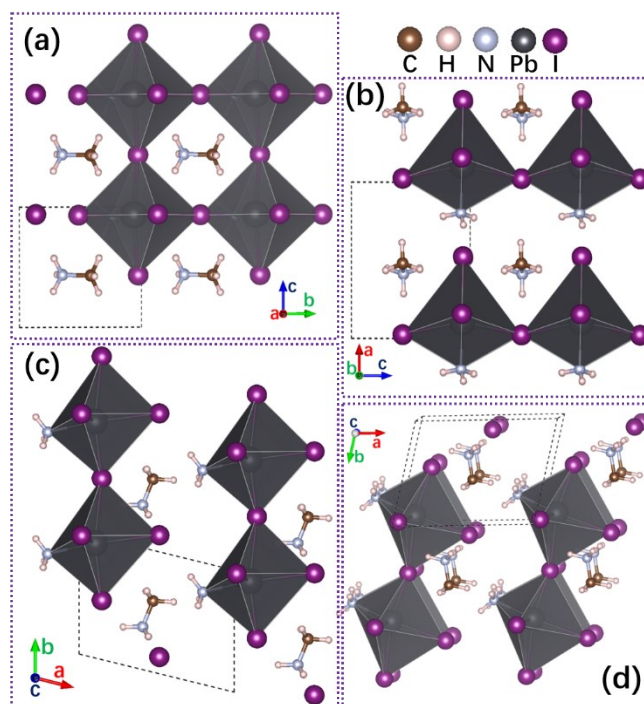


**Figure S10.** Structure of MPI-1NH<sub>3</sub>. Panel (a), (b) and (c) are top views from the *a*, *b* and *c* directions, respectively; (d) tilted view.

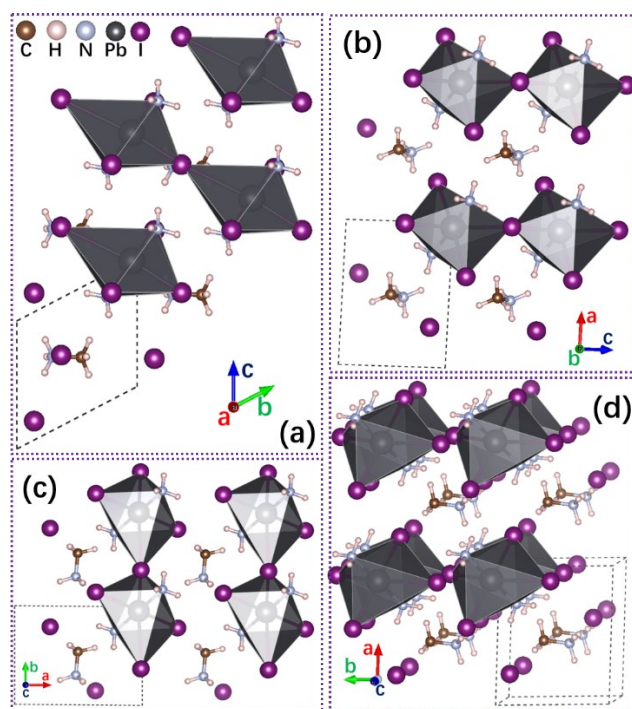


**Figure S11.** Structure of MPI-2NH<sub>3</sub>. Panel (a), (b) and (c) are top views from the *a*, *b* and *c* directions, respectively; (d) tilted view.

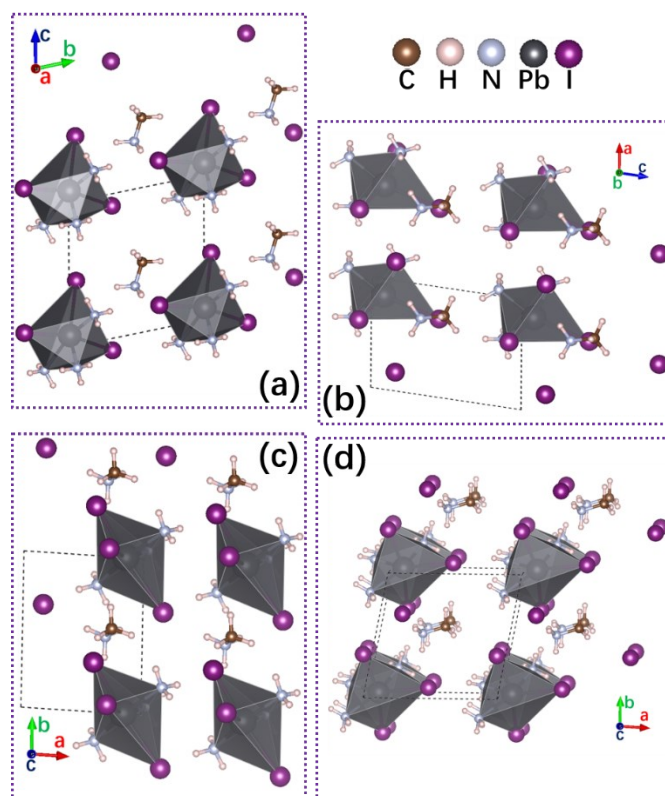


**Figure S12.** Structure of MPI-3NH<sub>3</sub>. Panel (a), (b) and (c) are top views from the *a*, *b* and *c* directions, respectively; (d) tilted view.

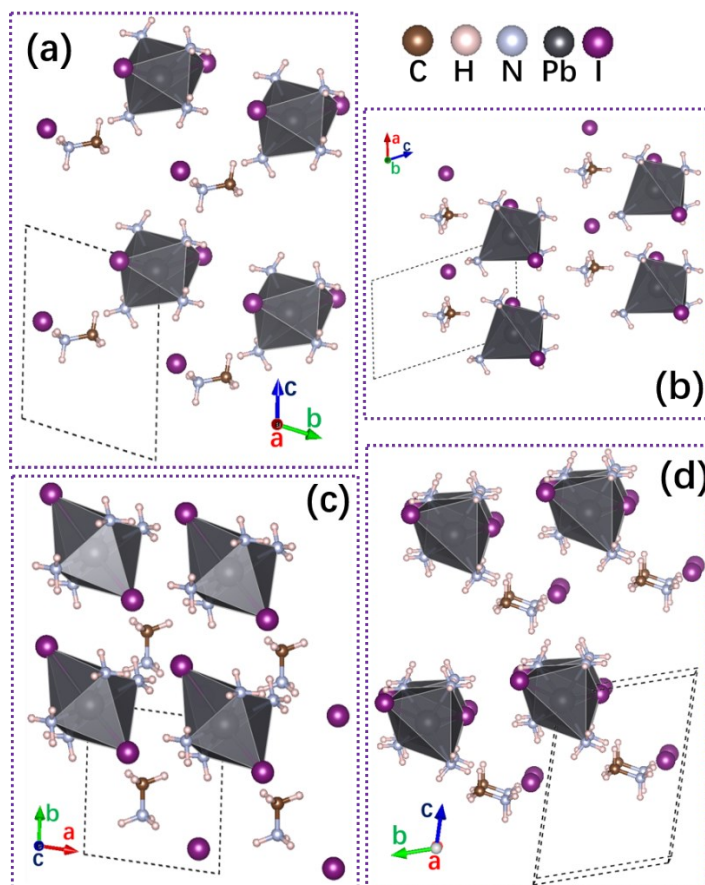


**Figure S13.** Structure of MPI-4NH<sub>3</sub>. Panel (a), (b) and (c) are top views from the *a*, *b* and *c* directions, respectively; (d) tilted view.

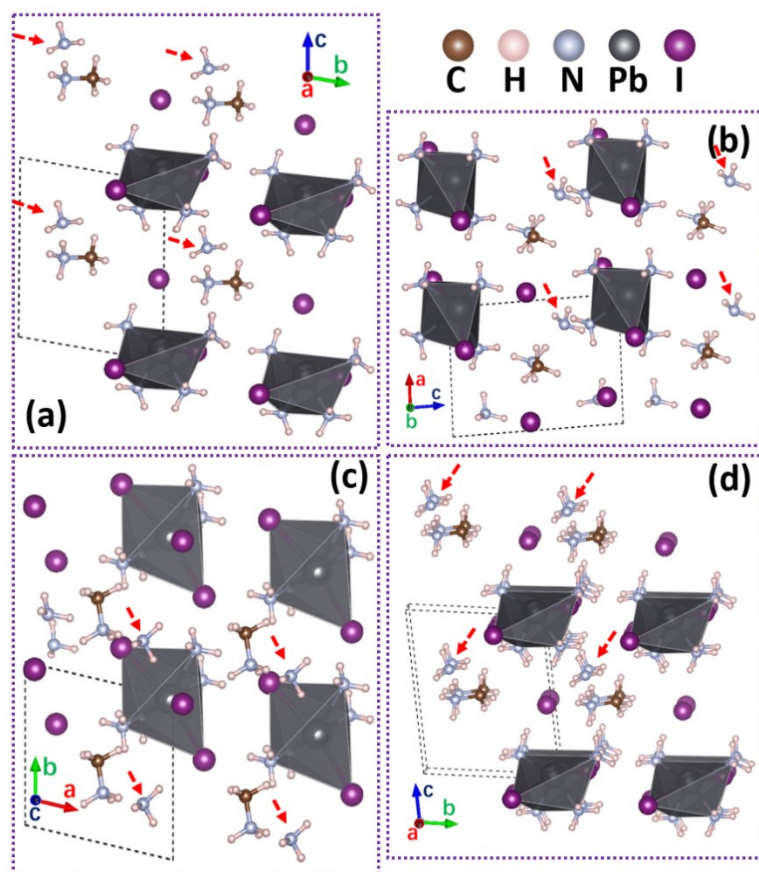


**Figure S14.** Structure of  $\text{MAPbI}_3\cdot 5\text{NH}_3$ . Panel (a), (b) and (c) are top views from the a, b and c directions, respectively; (d) tilted view. Red arrows point out the fifth  $\text{NH}_3$  molecular, which cannot bond with Pb because of the long distance between them.

The formation energy ( $E_f$ ) is calculated according to the equation (1). The details are below:

$$E_f = \frac{E_{(MAX+nNH_3)} - E_{MAX} - nE_{NH_3}}{n} \quad (1)$$

where MAX represent MPI, while  $E_{(MAX+nNH_3)}$ ,  $E_{MAX}$  and  $E_{NH_3}$  are the total energies of MPI-n(NH<sub>3</sub>), MPI, and NH<sub>3</sub> molecule, respectively, n is the number of NH<sub>3</sub> molecule. The corresponding calculated formation energy for the MPI-n(NH<sub>3</sub>) systems was shown in Table S3.

**Table S3.** Calculated formation energies of the MPI-n(NH<sub>3</sub>) systems, where n = 1, 2, 3, 4 and 5.

MPI-n(NH <sub>3</sub> )	n=1	n=2	n=3	n=4	n=5
Formation energy (eV/NH <sub>3</sub> )	0.374	0.284	0.289	0.358	0.329

The positive values of the formation energies indicate the formation processes are endothermic, whereas negative values suggest the reactions are exothermic. We see that the formation energies of all the MPI-n(NH<sub>3</sub>) systems are positive with values range from 0.284 to 0.358 eV/NH<sub>3</sub>, which mean the formation processes are endothermic. It is noted that a criterion of 0.1 eV/atom for exfoliation energy has been established from analysis of thousands of solids for formation of stable two-dimensional layers.<sup>12</sup> Our calculated formation energies range from 0.071 to 0.090 eV/atom, well below this criterion (0.1 eV/atom), suggesting the easy formation of the MPI-n(NH<sub>3</sub>) systems.

Small values of formation energies for the MPI-n(NH<sub>3</sub>) systems also indicate the reactions are reversible which is also consistent with our experimental finding.

## 7. References

- (1.) Feng, X.; Su, H.; Wu, Y.; Wu, H.; Xie, J.; Liu, X.; Fan, J.; Dai, J.; He, Z., Photon-generated carriers excite superoxide species inducing long-term photoluminescence enhancement of MAPbI<sub>3</sub> perovskite single crystals. *J. Mater. Chem. A* **2017**, *5*, 12048.
- (2.) Dang, Y. Y.; Liu, Y.; Sun, Y. X.; Yuan, D. S.; Liu, X. L.; Lu, W. Q.; Liu, G. F.; Xia, H. B.; Tao, X. T., Bulk crystal growth of hybrid perovskite material CH<sub>3</sub>NH<sub>3</sub>PbI<sub>3</sub>. *Crystengcomm* **2015**, *17*, 665.
- (3.) Li, Y.; Liu, F. Z.; Waqas, M.; Leung, T. L.; Tam, H. W.; Lan, X. Q.; Tu, B.; Chen, W.; Djurišić, A. B.; He, Z. B., Formamidinium-Based Lead Halide Perovskites: Structure, Properties, and Fabrication Methodologies. *Small Methods* **2018**, *2*, 1700387.
- (4.) Wu, Y.; Chen, W.; Lin, Y.; Tu, B.; Lan, X.; Wu, Z.; Liu, R.; Djurišić, A. B.; He, Z. B., General Method To Define the Type of Carrier Transport Materials for Perovskite Solar Cells via Kelvin Probes Microscopy. *ACS Appl. Energy Mater.* **2018**, *1*, 3984.
- (5.) Wu, Y. H.; Chen, W.; Chen, G.; Liu, L. Y.; He, Z. B.; Liu, R. C., The Impact of Hybrid Compositional Film/Structure on Organic-Inorganic Perovskite Solar Cells. *Nanomaterials* **2018**, *8*.
- (6.) Kresse, G.; Furthmüller, J., Efficient iterative schemes for ab initio total-energy calculations using a plane-wave basis set. *Phys. Rev. B* **1996**, *54*, 11169.
- (7.) Blöchl, P. E., Projector augmented-wave method. *Phys. Rev. B* **1994**, *50*, 17953.
- (8.) Perdew, J. P.; Burke, K.; Ernzerhof, M., Generalized Gradient Approximation Made Simple. *Phys. Rev. Lett.* **1996**, *77*, 3865.
- (9.) Monkhorst, H. J.; Pack, J. D., Special points for Brillouin-zone integrations. *Phys. Rev. B* **1976**, *13*, 5188.
- (10.) He, Y.; Galli, G., Perovskites for Solar Thermoelectric Applications: A First Principle Study of CH<sub>3</sub>NH<sub>3</sub>AI<sub>3</sub> (A = Pb and Sn). *Chem Mater* **2014**, *26*, 5394.
- (11.) Supplemental Material. <http://periodictable.com/Elements/053/data.html>

(12.) Ashton, M.; Paul, J.; Sinnott, S. B.; Hennig, R. G., Topology-Scaling Identification of Layered Solids and Stable Exfoliated 2D Materials. *Phys Rev Lett* **2017**, *118*, 106101.